Atmos. Chem. Phys. Discuss., 10, 18635–18659, 2010
www.atmos-chem-phys-discuss.net/10/18635/2010/
doi:10.5194/acpd-10-18635-2010

Atmospheric Chemistry and Physics Discussions

Stratocumulus cloud thickening beneath layers of absorbing smoke aerosol

E. M. Wilcox

Desert Research Institute, Reno, Nevada, USA

Received: 26 July 2010 – Accepted: 2 August 2010 – Published: 9 August 2010

Correspondence to: E. M. Wilcox (eric.wilcox@dri.edu)

Published by Copernicus Publications on behalf of the European Geosciences Union.

Stratocumulus cloud thickening beneath layers of absorbing smoke aerosol

E. M. Wilcox

Abstract

Marine stratocumulus cloud properties, and the free-tropospheric environment above them, are examined in NASA A-train satellite data for cases where smoke from seasonal burning of the West African savannah overlay the persistent southeast Atlantic stratocumulus cloud deck. CALIPSO space-borne lidar observations show that features identified as layers of aerosol occur predominantly between 2 km and 4 km altitude with double the frequency of occurrence of aerosol features in the boundary layer. Layers identified as cloud features occur predominantly below 1.5 km altitude and beneath the layer of elevated smoke aerosol. The diurnal mean shortwave heating rates attributable to the absorption of solar energy in the aerosol layer is nearly 1.5 K d^{-1} for an aerosol optical thickness value of 1, and increases to 1.8 K d^{-1} when the smoke resides above clouds owing to the additional component of upward solar radiation reflected by the cloud. As a consequence of this heating, the 700 hPa air temperature above the cloud deck is warmer by approximately 1 K on average for cases where smoke is present above the cloud compared to cases without smoke above cloud. The warmer conditions in the free-troposphere above the cloud during smoke events coincide with cloud liquid water path values that are greater by 20 g m^{-2} and cloud tops that are lower by approximately 50 m for overcast conditions compared to smoke-free periods. The observed thickening and subsidence of the cloud layer are consistent with published results of large-eddy simulations showing that solar absorption by smoke above stratocumulus clouds increases the buoyancy of free-tropospheric air above the temperature inversion capping the boundary layer. Increased buoyancy inhibits the entrainment of dry air through the cloud-top, thereby helping to preserve humidity and cloud cover in the boundary layer. The greater liquid water path for cases of smoke overlaying cloud implies a negative semi-direct radiative forcing of regional climate in locations such as the southeast Atlantic Ocean where absorbing aerosol layers frequently exist above persistent stratus cloud decks.

1 Introduction

The impact of aerosols upon the climate of Earth has received intense scrutiny because of the uncertain role aerosols play in present-day anthropogenic radiative forcing of climate (IPCC 2007), and the prospect for large present and future impacts of aerosol forcing on regional and global hydrological cycles (e.g. Ramanathan et al., 2001; Liepert et al., 2004). The radiative forcing by aerosols arises both through the direct scattering and absorption of solar radiation by aerosol particles, as well as the modification of clouds by aerosols, which can impact the transmission of solar and infrared radiation through the cloud layer.

In cases where absorbing aerosols (e.g. smoke and soot) coincide with clouds in the same column, the radiative heating of the troposphere by aerosol solar absorption may modify the thickness and coverage of the cloud layer depending on the radiative properties of the aerosol, the meteorology driving the cloud dynamics, and the vertical distribution of the aerosol relative to the cloud in the column. This so-called semi-direct effect of aerosols (Hansen et al., 1997) is often assumed to yield a positive radiative forcing (warming) of climate. When the absorbing aerosol mixes with shallow broken clouds in the same layer, the radiative heating of the layer by solar absorption can reduce the cloud cover (Ackerman et al., 2000), increasing the absorption of solar radiation at the surface and leading to a net positive radiative forcing.

This study examines the consequences for marine stratocumulus clouds of absorbing aerosol residing above the cloud-topped marine boundary layer. Seasonal burning of the southwestern African Savannah produces episodic plumes of dark smoke over the southeast Atlantic Ocean. Beneath the elevated layer of smoke is a persistent deck of bright marine stratocumulus cloud. Field measurements have verified that the smoke is substantially absorbing in the ultraviolet (UV) and visible wavelengths (Haywood et al., 2004), meaning that both the downward incident solar radiation from above, and the upward reflected solar radiation from the cloud-top below are substantially attenuated as solar energy is deposited in the smoke layer. The persistence of shallow

ACPD
10, 18635–18659, 2010

stratocumulus beneath deep plumes of absorbing smoke aerosol over the southeast Atlantic Ocean during the dry season provides a natural laboratory for testing the response of stratocumulus clouds to overlaying absorbing aerosol.

The geographical distribution of smoke from African Savannah burning, as well as the microphysical and radiative properties of the smoke, were among topics of study of the Southern African Regional Science Initiative (SAFARI) 2000 field campaign. During sampling offshore of West Africa, smoke was typically observed in layers that were vertically separated from stratocumulus clouds below (Hobbs, 2002; McGill et al., 2003). These observations imply that direct microphysical interaction between the aerosols and stratocumulus clouds is often inhibited by the strong temperature inversion above the cloud layer.

In large-eddy simulations of California stratocumulus cloud cases, Johnson et al. (2004) find that when the absorbing aerosol layer occurs in the boundary layer, the cloud liquid water path (LWP) decreases, yielding a positive semi-direct radiative forcing. However, when the aerosol layer occurs entirely above the boundary layer the temperature inversion above the boundary layer is enhanced, LWP increases, and the semi-direct radiative forcing is negative (a cooling). Evidence for both increases and decreases in cloud fraction associated with biomass burning aerosols offshore of California were reported by Brioude et al. (2009) depending on whether simulated smoke in a chemical transport model had mixed into the boundary layer or not. In this study we confirm the results of the Johnson et al. (2004) study for overcast decks of cloud to the presence of smoke above the boundary layer with an empirical analysis of a suite of NASA A-Train satellite observations and complementary radiative transfer calculations. The observations confirm that the smoke layer is often distinct from the cloud layer below and that a positive correlation of smoke loading and cloud liquid water path can be explained by warming of the cloud-capping temperature inversion attributable to solar absorption by smoke.

Discussion Paper | Discussion Paper | Discussion Paper | Discussion Paper |

ACPD

10, 18635–18659, 2010

Stratocumulus cloud thickening beneath layers of absorbing smoke aerosol

E. M. Wilcox

2 Data and methods

A combination of satellite observations and a numerical radiative transfer model are used to establish a link between absorbing smoke aerosol and a thickening of marine stratocumulus cloud beneath the smoke layer. Several of the satellite data sets employed, and the processing techniques applied to the satellite data, are similar to those described in Wilcox et al. (2009). Essential details are described below. Additional details and discussion can be found in Wilcox et al. (2009).

The vertical profile of smoke and cloud is determined using the aerosol and cloud feature mask derived from CALIOP lidar backscatter measurements from the CALIPSO satellite (Liu et al., 2009; Winker et al., 2009). A histogram of aerosol and cloud layer heights is used to construct a canonical profile for cases of coincident smoke aerosol overlaying cloud for input into the plane-parallel radiative transfer model of Chou (1992). Sensitivity studies are performed with the model to estimate the tropospheric heating rate for varying values of smoke aerosol optical depth (AOD) and cloud fraction.

The signature of tropospheric heating by absorbing smoke aerosol is observed in Atmospheric Infrared Sounder (AIRS) satellite tropospheric temperature products based on the AIRS/AMSU retrieval algorithm (Susskind et al., 2006). In order to properly interpret the AIRS temperatures, samples are sorted according to coincident observations of sea surface temperature (SST) from the Advanced Microwave Scanning Radiometer – EOS (AMSR-E) sensor (Wentz and Meissner, 2000; Wentz et al., 2003) and the aerosol index (AI) derived from the Ozone Monitoring Instrument (OMI) instrument (Herman et al., 1997; Ahmad et al., 2006). The AIRS and AMSR-E instruments are on the Aqua satellite and the OMI instrument is on the Aura satellite. The Aura satellite follows the Aqua satellite in the same orbit approximately 15 min behind. All data are taken from the daytime pass of the A-Train satellite constellation (approximately 01:30 p.m. local time).

The response of the clouds to tropospheric heating is determined using AMSR-E observations of cloud LWP (Wentz, 1997; Wentz and Spencer, 1998). We rely on the

ACPD
10, 18635–18659, 2010

AMSR-E LWP retrieval based on microwave emission rather than the higher resolution MODIS LWP retrieval based on visible and near-infrared reflectance because of a systematic bias in the MODIS LWP for cases where absorbing aerosol is present above the cloud (Haywood et al., 2004; Wilcox et al., 2009).

The satellite data are obtained for the oceanic region offshore of southern Africa bounded by 10 W to 15 E longitude and 20 S to 0 S latitude during July, August, and September (JAS). Aerosols emanating from the burning of the African savannah are clearly evident over this region of ocean in satellite imagery (Fig. 1a). All satellite data, with the exception of the CALIPSO data, are analyzed for the JAS period during 2005 and 2006. CALIPSO data are analyzed for the JAS period from 2006 through 2008. Instantaneous AMSR-E data are obtained for each orbit averaged in space on a 0.25° lat.-lon. grid. Level-2 AIRS pixel data are obtained at 45 km resolution, which is a broader spatial resolution than the grid. AIRS samples are colocated with the other data sets by obtaining the AIRS sample nearest the center point of the 0.25° grid cell. AIRS provides valid temperature retrievals even up to 90% cloud cover (Susskind et al., 2006). Many 0.25° grid cells confidently identified as overcast are collocated with valid AIRS retrievals. This likely indicates that for many cases some clear-sky regions are adjacent to the grid cell, yet within the broader AIRS footprint. Level-2 MODIS cloud pixel data (Platnick et al., 2003) are obtained at 1 km resolution and used to screen for overcast conditions as described below.

The AMSR-E gridded LWP is an average over the entire 0.25° area, including clear-sky portions of the grid cell. Therefore, the overcast LWP can only be obtained for grid cells confidently determined to be overcast. Because cloud thickening will be diagnosed by changes in LWP, and differences in LWP between broken cloud scenes can occur either because of differences in the thickness of the cloud layer or differences in cloud fraction, a stringent test for overcast conditions is made to isolate the thickening effect. Except where noted, only overcast grid cells are used in the analysis. This overcast screening is the same as applied operationally in the level-2 1-km MODIS visible/near-infrared cloud optical thickness and cloud drop effective radius product

ACPD
10, 18635–18659, 2010

(Platnick et al., 2003). In practice, the overcast screening is applied by only using grid cells completely spanned by MODIS 1-km samples with valid retrievals of cloud optical thickness and cloud drop effective radius flagged as "confident". This conservative screening for overcast conditions captures only about 30% of the overall cloud cover because many clouds are smaller than a grid cell. However, there remain greater than 47 000 overcast grid cells with valid coincident SST, LWP, and OMI AI values in two years of daytime satellite overpasses during the JAS period.

The OMI AI is used to estimate the column amount of smoke residing above the cloud. While this data set provides a high spatial resolution, quantitative indication of the amount of smoke residing above clouds for the entire Aqua observing period, even for overcast conditions, the magnitude of the AI is dependent on the optical properties and vertical distribution of the aerosols, even if the column amount of aerosol is unchanged. Having little knowledge of the variability of aerosol optical properties in our study, it is not possible to quantitatively assess the uncertainties related to this variability in our application of the AI data. Variations in the vertical distribution of aerosols, however, is not a likely source of significant error in using the OMI AI as a proxy for smoke loading above clouds. Torres et al. (1998) find that variations in the altitude of absorbing aerosol over a range of approximately 5 km have little impact on ultraviolet radiance for cases with a surface reflectance of 0.6, a value consistent with measured UV reflectance for liquid water clouds (Eck et al., 1987).

A summary of observing systems used in this study appears in Table 1, including values of reported uncertainties in instantaneous parameter retrievals from the literature estimated from the RMS error of retrievals performed at instrument resolution.

3 The radiative effect of smoke aerosol

Smoke aerosols from African savannah burning directly heat the atmospheric layer in which they reside owing to absorption of solar radiation (Pilewskie et al., 2003; Magi et al., 2008). Calculations with the plane-parallel radiative transfer model of Chou (1992) are performed in order to illustrate the radiative consequences of a thick layer

ACPD
10, 18635–18659, 2010

of absorbing aerosol overlaying a low cloud deck. Of particular interest are the vertical distribution of the aerosol in relation to the cloud-topped boundary layer, and the resulting vertical profile of atmospheric heating. Profiles of aerosol and cloud features, determined statistically from the CALIPSO satellite measurements, are used to constrain the radiative transfer calculations and determine where in the column to expect the thermal signature of the aerosol radiative warming.

In the lower troposphere the CALIOP lidar identifies aerosol and cloud features at 30 m vertical resolution and 333 m horizontal resolution. The vertical number distribution of all daytime aerosol features identified during the JAS period from 2006 through 2008 is shown in Fig. 1b. All daytime CALIPSO passes through the box shown in Fig. 1a are accumulated in the profile shown in Fig. 1b and c. Although the sensitivity of CALIOP to detecting aerosol and cloud features is weaker for the daylight portions of CALIPSO orbits (Winker et al., 2009), only daytime passes are used here to determine the smoke profile when solar absorption is occurring. The presence of aerosol features clearly peaks between 2 km and 4 km, indicating that the smoke is preferentially transported from the continent to the southeastern Atlantic ocean in plumes between those altitudes. Aerosol features in the boundary layer are substantially smaller in number than at 3 km. The occurrence of boundary layer aerosol features is underestimated in Fig. 1b relative to the abundance of features above the boundary layer because clouds at the top of the boundary layer fully attenuate the lidar beam some of the time. However, when the data are screened for cases where the beam penetrates to the surface, the number of aerosol features at 3 km exceeds the number of boundary layer features by greater than a factor of 2 (not shown).

The number distribution of all aerosol and cloud features is shown in Fig. 1c. The stratocumulus clouds occur predominantly between 0.5 km and 1.3 km. A distinct minimum in aerosol and cloud features occurs between the stratocumulus cloud layer and the elevated smoke aerosol layer. Based on these results, a representative profile with a single layer of elevated absorbing aerosols and single layer of shallow clouds below is imposed in the radiative transfer model (Fig. 2).

ACPD
10, 18635–18659, 2010

Stratocumulus cloud thickening beneath layers of absorbing smoke aerosol

E. M. Wilcox

The model simulates scattering and absorption of shortwave radiation in a single column by aerosols, clouds, ozone, water vapor, oxygen, and carbon dioxide in 75 pressure levels from the surface to the top of the atmosphere. Each layer is approximately 24 hPa thick in the lower and middle troposphere. The vertical distribution of AOD in each model layer is shown in Fig. 2a for the case of total column optical thickness of value 1. The aerosols are distributed in a half-sinusoidal profile from 1.5 km to 4.2 km altitude with peak aerosol concentration at about 3 km altitude. Aerosol optical properties are derived from in-situ observations during the SAFARI 2000 field campaign (Haywood et al., 2003) where it is reported that the single-scatter albedo was 0.89 at 0.55 µm. Simulated clouds are in a single layer from 0.5 km to 1.25 km altitude with uniform liquid water mixing ratio of 0.07 g kg^{-1} yielding a cloud of total optical thickness of 12.

The diurnal mean shortwave radiative heating rate profile is shown in figure 2b for cases of AOD equal to 0, 0.4, and 1.0 and cloud fraction of 1. In the absence of smoke aerosol the lower tropospheric shortwave heating rate is about 1 K d^{-1}. For smoke and cloud profiles constrained by CALIPSO observations the radiative heating rate peaks between the 600 and 700 hPa pressure levels. The peak heating rate in the aerosol layer is 2 K d^{-1} and 3.5 K d^{-1} for AOD of 0.4 and 1.0 respectively.

The difference between the solid line in Fig. 2b and the other lines is the shortwave heating rate attributable to aerosol absorption. The aerosol shortwave heating rate for cloud-free conditions and averaged over the aerosol layer is shown as a function of AOD from 0 to 1 in Fig. 3 (solid line). The layer-mean aerosol heating rate increases from 0 for no aerosol to just less than 1.5 K d^{-1} for AOD = 1. The aerosol shortwave heating rate increases with cloud fraction because the smoke aerosol absorbs both the downwelling solar radiation and the upwelling solar radiation reflected by the cloud beneath the aerosol. For the AOD = 1 case, the aerosol shortwave heating rate increases from just less than 1.5 K d^{-1} for cloud-free conditions to 1.8 K d^{-1} for overcast conditions.

ACPD
10, 18635–18659, 2010

The aerosol shortwave heating rate for AOD = 1 corresponds to a radiative flux convergence in the atmosphere of 42 W m^{-2} for cloud-free conditions and 57 W m^{-2} for overcast conditions. The radiative forcing efficiency in the atmosphere reported by Magi et al. (2008) based on a more rigorous application of SAFARI 2000 observations and a radiative transfer model is 70.3 +/– 5.1 W m^{-2} $\tau_{550\,\mathrm{nm}}{}^{-1}$. Therefore it is likely that the atmospheric heating rates in Figs. 2 and 3 may be underestimated. The Magi et al. (2008) results are calculated over continental sites, and therefore their clear-sky radiative forcing efficiency is based on a higher surface reflectance. Furthermore, the Magi et al. (2008) study accounts for spatio-temporal variability in aerosol radiative properties. An observed negative correlation between aerosol single-scattering albedo and AOD will lead to an enhanced atmospheric radiative forcing efficiency that is not accounted for here.

4 Smoke absorption and lower tropospheric air temperature

The AIRS air temperature retrievals at the 700 and 600 hPa pressure levels are shown in Fig. 4 binned by AMSR-E SST. Vertical bars in Figs. 4 and 5 indicate the 95% confidence interval estimated as plus/minus double the standard deviation of the mean of all samples in each SST bin. In the absence of reliable boundary layer air temperature, SST is used here as a general indicator of boundary layer temperature. While LWP increases strongly with SST in this region, as discussed further below, there is no apparent relationship between free-tropospheric temperature above the boundary layer and SST. The data are further stratified by clean and polluted conditions, where clean conditions are indicated by OMI AI less than 1 and polluted conditions are indicated by OMI AI greater than 2. At the 700 hPa pressure level, approximately the level of peak aerosol shortwave radiative heating, polluted samples are systematically warmer than clean samples by nearly 1 K. This is true regardless of SST except for those samples at the edges of the SST distribution. However, less than 8% of samples are associated with SST less than 290 K or greater than 298 K. The cloud LWP data discussed below is limited only to overcast samples. The AIRS retrievals, however, are available for clear or overcast conditions. Figure 5 indicates that the polluted scenes are warmer at 700 hPa than the clean scenes regardless of cloud cover.

Estimates of heating rates by dynamical processes at 700 hPa are found to be substantially smaller than the aerosol shortwave heating rates estimated above. Horizontal temperature advection and subsidence heating are derived from the temperature and wind fields from the NCEP reanalysis data (Kalnay et al., 1996) for clean and polluted samples (not shown). The sum of the differences between clean and polluted conditions for the components of dynamical heating are less than 0.5 $\mathrm{K\,d^{-1}}$, suggesting that much of the difference in AIRS temperatures at this level between clean and polluted conditions is attributable to the shortwave radiative heating.

At the 600 hPa pressure level, near the top of the smoke layer where shortwave aerosol heating rates are low, there is no systematic difference between clean and polluted scenes, except for the 30% of samples with SST cooler than 293 K, where the clean samples are on average warmer than the polluted samples.

5 Lower tropospheric warming and cloud thickening

Cloud LWP increases strongly with SST as shown in Fig. 5a. This positive correlation may suggest that higher SSTs promote cloud cover through greater fluxes of heat and moisture from the surface to the boundary layer. This characterizes the response of clouds to changes of SST on short time scales of a day or less (Pincus et al., 1997). But given the non-local effects of SSTs and static stability upwind on local cloud development (Klein et al., 1995), proper characterization of the relationship between SST and LWP requires a Lagrangian analysis. Nevertheless, regardless of the SST, Fig. 5a indicates that LWP is systematically greater by approximately 20 $\mathrm{g\,m^{-2}}$ for overcast polluted scenes compared to the clean scenes. These results are consistent with the large-eddy simulation results presented by Johnson et al. (2004) where simulations of a stratocumulus cloud layer overlain by a layer of absorbing biomass burning aerosol resulted in LWP values of 5 to 10 $\mathrm{g\,m^{-2}}$ greater than in a simulation without the biomass burning aerosol layer.

ACPD
10, 18635–18659, 2010

The Johnson et al. (2004) simulations indicate that the increase in the buoyancy of the layer immediately above the cloud owing to warming by solar absorption reduces cloud-top entrainment. Reduced entrainment of dry air through the cloud-top acts to preserve humidity and cloud cover in the boundary layer. The result is a shallower boundary layer with greater LWP in the cloud layer.

The shallower boundary layer is indicated in the frequency of occurrence of CALIPSO cloud features sorted by OMI AI (Fig. 5b). The relative frequency of occurrence of cloud features for high smoke and low smoke conditions is shown separately as the ratio of the number of features in each 30 m layer in the CALIPSO lower-tropospheric feature mask product and the total number of either high-smoke or low-smoke features detected below 2.5 km altitude. In the upper portion of the cloud layer, between 1 km and 1.5 km altitude, the distribution of cloud tops under low smoke conditions is higher than for clouds under high smoke conditions. Subsidence of the cloud deck accompanies subsidence of the free-troposphere above. The altitude of the cloud top is determined by a balance between the subsidence above the boundary layer and the vertical entrainment at cloud-top. With the reduction in entrainment implied by the warmer free-tropospheric air above the inversion when smoke is present, subsidence of the cloud-top accompanies the continued subsidence in the free-troposphere above. The frequency distributions of CALIPSO cloud features suggest that the enhanced subsidence of the cloud tops may be only 30 to 50 m, which is similar in magnitude to the subsidence in simulated clouds for smoke-over-cloud conditions reported by Johnson et al. (2004), and is also near the detection limit of CALIPSO. The subsidence of the cloud-top is also indicated in greater cloud-top pressure and greater cloud-top temperature values in the MODIS data for high smoke conditions for all values of SST. However, these values are determined from a combination of the observed infrared radiances and simulated temperature profiles from an atmospheric analysis data product which has known deficiencies in resolving strong temperature inversions (Harshvardhan et al., 2009), therefore the MODIS products may not reliably capture the magnitude of cloud-top subsidence in this region of strong inversions above the

ACPD
10, 18635–18659, 2010

boundary layer. Indeed, the difference in cloud-top pressure between high-smoke and low-smoke conditions implied by MODIS is substantially greater in magnitude than is indicated in the CALIPSO data.

Increases in LWP associated with increases in aerosol load are often attributed to a microphysical interaction whereby aerosols entrained into the cloud layer suppress drizzle (Albrecht, 1989). Often this effect is argued to yield an increase in area-averaged LWP through an increase in cloud cover. Only overcast LWP is addressed in the present study. Hence, the increase in LWP attributed here to the smoke aerosol is a geometric thickening or an increase the liquid water content of the cloud. A significant microphysical response of the clouds to the smoke is not expected based on the CALIPSO analysis presented above and the SAFARI 2000 results (e.g. Hobbs, 2002) indicating clear air often occurs beneath the smoke layers. This is further confirmed by Costantino and Bréon (2010) who find that 83% of CALIPSO profiles, out of more than 7000 examined in the same region, have a vertical profile where the aerosol and cloud layers are separated by at least 250 m. If substantial microphysical interactions between the smoke layer and cloud layer are occurring then a negative correlation between aerosol load and cloud drop effective radius would be expected. Examination of the MODIS data indicates that the effective cloud drop radius retrieved for the high smoke cases is smaller than that of the low smoke cases by approximately 1 µm. However, the radiative impact of the smoke above the cloud introduces a low bias of less than 2 µm in the MODIS retrievals of effective radius (Haywood et al., 2004), which could account for the difference observed here. Costantino and Bréon (2010) confirm that the inverse relationship between cloud drop effective radius with aerosol load in satellite data is substantially weaker for cases where the smoke and cloud layers are physically separated compared to cases where the vertical separation is small and microphysical interaction is likely. These results suggest that the increase in LWP observed in this study is more likely a response to the warming above the cloud layer than a microphysical interaction of aerosol entrained into the cloud.

ACPD
10, 18635–18659, 2010

A layer of absorbing aerosol over a bright cloud layer will darken the scene as viewed from above owing to the absorption of both downwelling solar radiation and upwelling reflected solar radiation. Podgorny and Ramanathan (2001) describe how the direct radiative forcing of scenes containing both absorbing aerosols and low clouds depends upon cloud fraction based on radiative transfer modeling. They find that the direct aerosol radiative forcing at the top-of-atmosphere changes from negative to positive as cloud cover increases. The level of cloud cover corresponding to the change in sign of the forcing depends on the aerosol optical thickness, aerosol single-scattering albedo, and whether the aerosol layer resides above the cloud or in the cloud. Chand et al. (2009) determine that this critical cloud fraction is about 0.4 for the southeast Atlantic region considered here based on satellite remote sensing observations. Therefore, the direct radiative forcing at the top-of-atmosphere of the smoke aerosol is expected to be positive for the overcast scenes explored here. However, the albedo of low clouds increases with LWP, therefore the thickening of the stratocumulus cloud in response to overlaying smoke aerosol is expected by yield a negative semi-direct radiative forcing that counteracts the positive aerosol direct radiative forcing. In the Johnson et al. (2004) simulations of the case of absorbing aerosol over cloud these two forcing effects nearly cancel. As noted above, however, this balance will depend on the amount and optical properties of both the aerosols and the cloud. Therefore, the cancelation of the two forcing effects should not be expected to hold for all cases of aerosol over low clouds.

This study has focused specifically on the increase of overcast LWP attributable to aerosol direct heating above the cloud. Increased stability of the lower troposphere may also increase the coverage of stratocumulus cloud as implied by the spatio-temporal correlation of lower tropospheric static stability and cloud cover (Klein and Hartmann, 1993). This effect would contribute an additional negative radiative forcing.

6 Summary

The stratocumulus clouds capping the marine boundary in the Southeast Atlantic Ocean frequently reside below an elevated layer of smoke aerosol transported off-shore from the regions of African Savannah burning. This study has investigated the radiative impact of the smoke on the atmospheric temperature in the free-troposphere above the marine boundary layer, and the properties of overcast samples of the clouds capping the marine boundary layer.

Analysis of CALIPSO satellite lidar data indicate that the smoke over the ocean primarily resides between 2 km and 4 km altitude, while the stratocumulus cloud decks generally reside below 1.5 km altitude. Radiative transfer calculations based on the observed profile and aerosols and clouds, as well as aerosol optical properties available from the literature, show that the presence of the smoke layer leads to a broad layer of heating in the lower troposphere that peaks near the 700 hPa pressure level. Mean shortwave radiative heating in the aerosol layer for cloud-free conditions exceeds $1\ \mathrm{K\,d^{-1}}$ for AOD values greater than about 0.5 and exceeds $1.5\ \mathrm{K\,d^{-1}}$ for AOD of 1. A small enhancement of the layer-mean heating rate occurs when clouds are present beneath the smoke owing the additional upwelling component of solar radiation reflected from the cloud-top.

AIRS satellite retrievals of atmospheric temperature indicate that the temperature at 700 hPa is warmer by nearly 1 K for cases where smoke is present above the cloud compared to cases with little or no smoke above the cloud. Differences in the dynamical heating rates estimated from NCEP reanalysis between high-smoke and low-smoke conditions are considerably smaller than the aerosol radiative heating rates estimated above, indicating that the aerosols are more important than dynamics for modifying the temperature above the cloud-top inversion. The warm conditions above the cloud layer coincide with LWP values for overcast conditions that are greater for high smoke cases by more than $20\ \mathrm{g\,m^{-2}}$ compared to low smoke or smoke-free cases, and cloud tops are lower by approximately 50 m. The smoke layer is typically separated vertically from

ACPD
10, 18635–18659, 2010

the cloud layer; hence little evidence is found for microphysical interactions between the smoke particles and the cloud layer. Therefore the thickening and subsidence of the cloud layer are attributed to the warming above the cloud-top. Warming in this layer increases the buoyancy of the free-tropospheric air above the cloud and inhibits entrainment of that air into the cloud layer. As indicated by cloud modeling studies, reduced drying by entrainment enhances LWP in the cloud and promotes subsidence of the cloud-top. The satellite data presented in this study indicate that this semi-direct thickening of cloud in response to the radiative effects of absorbing smoke aerosols is occurring during the dry season over the Southeast Atlantic Ocean.

The direct radiative effect of absorbing aerosols residing over a bright cloud deck is a positive radiative forcing (warming) at the top of the atmosphere. However, the semi-direct thickening of the cloud layer is a negative radiative forcing (cooling) owing to the enhanced albedo of thicker clouds. The balance of these opposing radiative forcing effects will depend on the amount and optical properties of the aerosol, as well as the optical thickness and fractional coverage of the cloud deck.

Acknowledgements. This work was supported by the NASA Radiation Sciences Program. AMSR-E data are produced by Remote Sensing Systems and sponsored by the NASA Earth Science REASoN DISCOVER Project and the AMSR-E Science Team. These data are available at www.remss.com. OMI and AIRS data are distributed by the Goddard Earth Sciences Data and Information Services Center. MODIS atmosphere products are distributed by the MODIS Adaptive Processing System at NASA GSFC. CALIPSO data are distributed by the Atmospheric Science Data Center at NASA Langley.

References

Ackerman, A. S., Toon, O. B., Stevens, D. E., Heymsfield, A. J., Ramanathan, V., and Welton, E. J.: Reduction of tropical cloudiness by soot, Science, 288, 1042–1047, 2000.

Ahmad, S. P., Torres, O., Bhartia, P. K., Leptoukh, G., and Kempler, S.: Aerosol index from TOMS and OMI measurements, Proceedings of the 14th AMS conference on the Applications of Air Pollution Meteorology with the Air and Waste Management Assoc., 2006.

Albrecht, B. A.: Aerosols, Cloud Microphysics, and Fractional Cloudiness, Science, 245, 1227–1230, 1989.
Brioude, J., Cooper, O. R., Feingold, G., Trainer, M., Freitas, S. R., Kowal, D., Ayers, J.K., Prins, E., Minnis, P., McKeen, S. A., Frost, G. J., and Hsie, E.-Y.: Effect of biomass burning on marine stratocumulus clouds off the California coast, Atmos. Chem. Phys., 9, 8841–8856, doi:10.5194/acp-9-8841-2009, 2009.
Chand, D., Wood, R., Anderson, T. L., Satheesh, S. K., and Charlson, R. J.: Satellite-derived direct radiative effect of aerosols dependent on cloud cover, Nat. Geosci., 2, 181–184, 2009.
Chou, M. D.: A solar radiation model for use in climate studies, J. Atmos. Sci., 49, 762–772, 1992.
Costantino, L. and Bréon, F.-M.: Analysis of aerosol-cloud interaction from multi-sensor satellite observations, Geophys. Res. Lett., 37, L11801, doi:10.1029/2009GL041828, 2010.
Eck, T. F., Bhartia, P. K., Hwang, P. H., and Stowe, L. L.: Reflectivity of Earth's surface and clouds in ultraviolet from satellite observations, J. Geophys. Res., 92, 4287–4296, 1987.
Harshvardhan, Zhao, G., Di Girolamo, L., and Green, R. N.: Satellite-observed location of stratocumulus cloud-top heights in the presence of strong inversions, IEEE T. Geosci. Remote, 47, 1421–1428, 2009.
Hansen, J., Sato, M., and Ruedy, R.: Radiative forcing and climate response, J. Geophys. Res., 102, 6831–6864, 1997.
Haywood, J. M., Francis, P., Dubovik, O., Glew, M., and Holben, B.: Comparison of aerosol size distributions, radiative properties, and optical depths determined by aircraft observations and Sun photometers during SAFARI 2000, J. Geophys. Res., 108, 8471, doi:10.1029/2002JD002250, 2003.
Haywood, J. M., Osborne, S. R., and Abel, S. J.: The effect of overlying absorbing aerosol layers on remote sensing retrievals of cloud effective radius and cloud optical depth, Q. J. Roy. Meteorol. Soc., 130, 779–800, 2004.
Herman, J. R., Bhartia, P. K., Torres, O., Hsu, C., Seftor, C., and Celarier, E.: Global distribution of UV-absorbing aerosols from Nimbus 7/TOMS data, J. Geophys. Res., 102, 16911–16922, 1997.
Hobbs, P. V.: Clean air slots amid atmospheric pollution, Nature, 415, p. 861, 2002.
Johnson, B. T., Shine, K. P., and Forster, P. M.: The semi-direct aerosol effect: impact of absorbing aerosols on marine stratocumulus, Q. J. Roy. Meteorol. Soc., 130, 1407–1422, 2004.

ACPD
10, 18635–18659, 2010

Stratocumulus cloud thickening beneath layers of absorbing smoke aerosol

E. M. Wilcox

Klein, S. A. and Hartmann, D. L.: The seasonal cycle of low stratiform clouds, J. Climate, 6, 1587–1606, 1993.
Klein, S. A, Hartmann, D. L., and Norris, J. R.: On the relationships among low-cloud structure, sea surface temperature, and atmospheric circulation in the summertime northeast Pacific, J. Climate, 8, 1140–1155, 1995.
Liepert, B., Feichter, J., Lohmann, U., and Roeckner, E. : Can aerosols spin down the water cycle in a warmer and moister world?, Geophys. Res. Lett., 31, L06207, doi:10.1029/2003GL019060, 2004.
Liu, Z., Vaughan, M., Winker, D., Kittaka, C., Getzewich, B., Kuehn, R., Omar, A., Powell, K., Trepte, C., and Hostetler, C.: The CALIPSO lidar cloud and aerosol discrimination: Version 2 algorithm and initial assessment of performance, J. Atmos. Oceanic Technol., 26, 1198–1213, 2009.
Magi, B. I., Fu, Q., Redemann, J., and Schmid, B.: Using aircraft measurements to estimate the magnitude and uncertainty of the shortwave direct radiative forcing of southern African biomass burning aerosol, J. Geophys. Res., 113, D05213, doi:10.1029/2007JD009258, 2008.
McGill, M. J., Hlavka, D. L., Hart, W. D., Welton, E. J., and Campbell, J. R.: Airborne lidar measurements of aerosol optical properties during SAFARI-2000, J. Geophys. Res., 108, 8493, doi:10.1029/2002JD002370, 2003.
Pilewskie, P., Pommier, J., Bergstrom, R., Gore, W., Howard, S., Rabbette, M., Schmid, B., Hobbs, P. V., and Tsay, S. C.: Solar spectral radiative forcing during the Southern African Regional Science Initiative, J. Geophys. Res., 108, 8486, doi:10.1029/2002JD002411, 2003.
Pincus, R., Baker, M. B., and Bretherton, C. S.: What controls stratocumulus radiative properties?, Lagrangian observations of cloud evolution, J. Atmos. Sci., 54, 2215–2236, 1997.
Platnick, S., King, M. D. Ackerman, A., Menzel, W. P., Baum, B. A. Riédi, J. C., and Frey, R. A.: The MODIS cloud products: algorithms and examples from Terra, IEEE T. Geosci. Remote, 41, 459–473, 2003.
Podgorny, I. A. and Ramanathan, V.: A modeling study of the direct effect of aerosols over the tropical Indian Ocean, J. Geophys. Res., 106, 24097–24105, 2001.
Ramanathan, V., Crutzen, P. J., Kiehl, J. T., and Rosenfeld, D.: Aerosols, climate, and the hydrological cycle, Science, 294, 2119–2124, 2001.
Susskind, J., Barnet, C., Blaisdell, J., Iredell, L., Keita, F., Kouvaris, L., Molnar, G., and Chahine, M.: Accuracy of geophysical parameters derived from Atmospheric Infrared

ACPD
10, 18635–18659, 2010

Stratocumulus cloud thickening beneath layers of absorbing smoke aerosol

E. M. Wilcox

Sounder/Advanced Microwave Sounding Unit as a function of fractional cloud cover, J. Geophys. Res., 111, D09S17, doi:10.1029/2005JD006272, 2006.
Torres, O., Bhartia, P. K., Herman, J. R., Ahmad, Z., and Gleason, J.: Derivation of aerosol properties from satellite measurements of backscattered ultraviolet radiation: theoretical basis, J. Geophys. Res., 103, 17099–17110, 1998.
Wentz, F. J.: A well-calibrated ocean algorithm for Special Sensor Microwave/Imager, J. Geophys. Res., 102, 8703–8718, 1997.
Wentz, F. J. and Spencer, R. W.: SSM/I rain retrievals within a unified all-weather ocean algorithm, J. Atmos. Sci., 55, 1613–1627, 1998.
Wentz, F. J. and Meissner, T.: AMSR Ocean Algorithm, Version 2, report number 121599A-1, Remote Sensing Systems, Santa Rosa, CA, 66 pp., available at: www.remss.com, 2000.
Wentz, F. J., Gentemann, C. L., and Ashcroft, P. D.: On-orbit calibration of AMSR-E and the retrieval of ocean products, paper presented at the 12th Conference on Satellite Meteorology and Oceanography, Am. Meteorol. Soc., Long Beach, Calif., available at: www.remss.com, 2003.
Wilcox, E. M., Roberts, G., and Ramanathan, V.: Influence of aerosols on the shortwave cloud radiative forcing from north Pacific Oceanic Clouds: Results from the Cloud Indirect Forcing Experiment (CIFEX), Geophys. Res. Lett., 33, L21804, doi:10.1029/2006GL027150, 2006.
Wilcox, E. M., Harshvardhan, and Platnick, S.: Estimate of the impact of absorbing aerosol over cloud on the MODIS retrievals of cloud optical thickness and effective radius using two independent retrievals of liquid water path, J. Geophys. Res., 114, D05210, doi:10.1029/2008JD010589, 2009.
Winker, D. M., Vaughan, M. A., Omar, A., Hu, Y., Powell, K. A., Liu, Z., Hunt, W. H., and Young, S. A.: Overview of the CALIPSO Mission and CALIOP Data Processing Algorithms, J. Atmos. Oceanic Technol., 26, 2310–2323, 2009.

ACPD
10, 18635–18659, 2010

Stratocumulus cloud thickening beneath layers of absorbing smoke aerosol

E. M. Wilcox

Table 1. Data sources.

Parameter	Sensor	Platform	Units	RMS uncertainty
aerosol/cloud feature	CALIOP	CALIPSO	n/a	n/a
Aerosol index	OMI	Aura	n/a	n/a
SST	AMSR-E	Aqua	K	0.76 K[§]
LWP	AMSR-E	Aqua	$g\,m^{-2}$	25 $g\,m^{-2}$[*]
Air temperature	AIRS	Aqua	K	1.5 K[†]
Cloud cover	MODIS	Aqua	n/a	n/a

Estimated uncertainties are reported RMS error of retrieved parameter at instrument resolution. [§]Wentz et al. (2003); [*]Wentz (1997); [†]Susskind et al. (2007).

ACPD
10, 18635–18659, 2010

Stratocumulus cloud thickening beneath layers of absorbing smoke aerosol

E. M. Wilcox

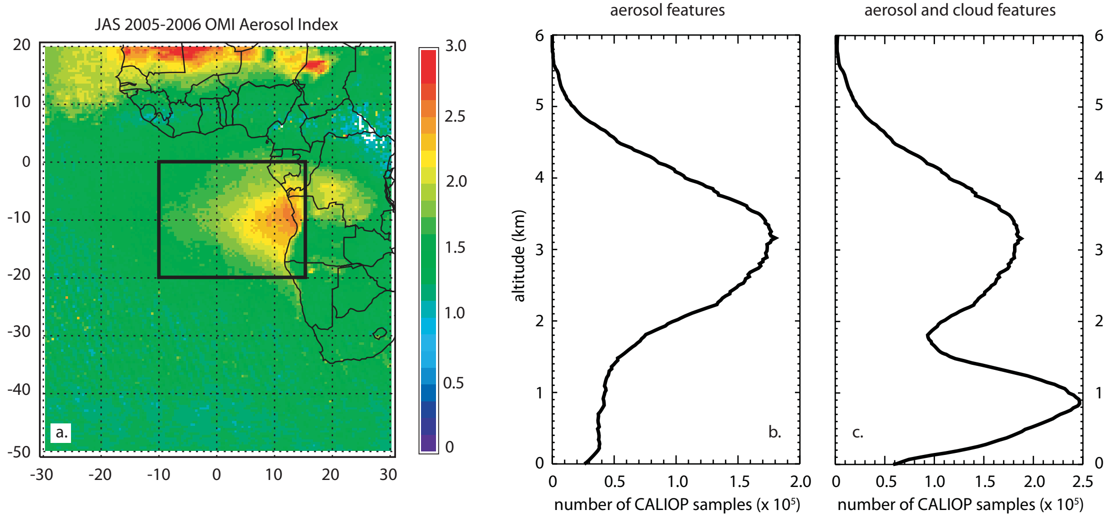

Fig. 1. **(a)** 2005–2006 July, August, and September average OMI aerosol index (from: Wilcox et al., 2009). **(b)** Vertical distribution of aerosol features, and **(c)** vertical distribution of aerosol and cloud features. Aerosol and cloud features from the CALIPSO feature mask product.

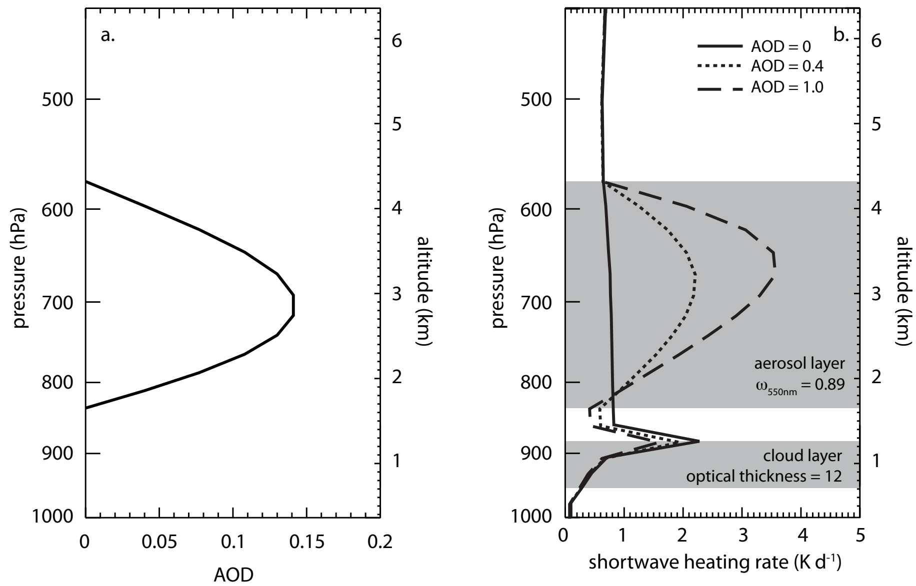

Fig. 2. (a) The vertical profile of aerosol optical depth (AOD) in each 24 hPa layer of the radiative transfer model for the case with total column optical depth of 1.0. **(b)** Simulated atmospheric shortwave heating rates for smoke layers of AOD = 0, 0.4, and 1.0 above a stratocumumlus cloud layer of optical thickness 12.

ACPD
10, 18635–18659, 2010

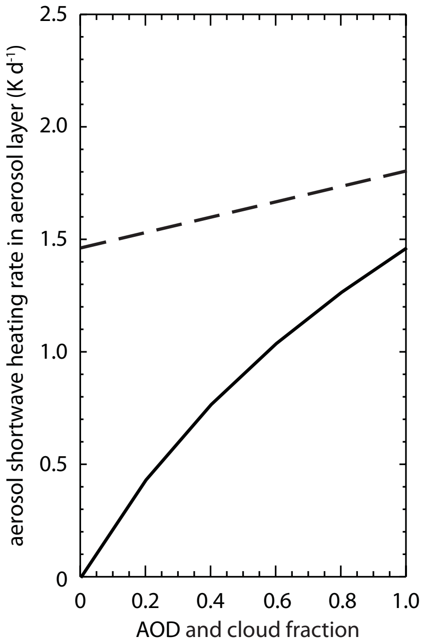

Fig. 3. Atmospheric shortwave heating rate averaged over the simulated smoke layer (1700–4300 m). Heating rate vs. AOD indicated by the solid line and the dashed line shows the heating rate for AOD = 1.0 vs. fraction of cloud cover beneath the smoke layer.

ACPD
10, 18635–18659, 2010

Title Page
Abstract | Introduction
Conclusions | References
Tables | Figures
Back | Close
Full Screen / Esc
Printer-friendly Version
Interactive Discussion

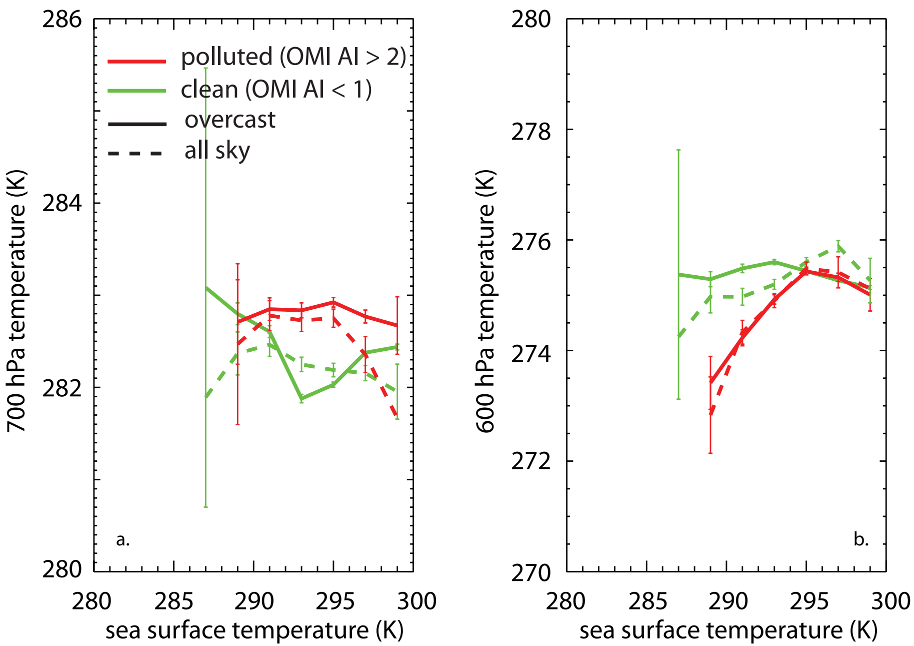

Fig. 4. AIRS atmospheric temperature at the **(a)** 700 hPa pressure level and **(b)** 600 hPa pressure level against AMSR-E sea surface temperature for high smoke and low smoke samples. Air temperatures are shown separately for overcast samples only (solid lines), and for all samples (dashed). Vertical bars are the estimated 95% confidence interval based on variability in each SST bin.

ACPD
10, 18635–18659, 2010

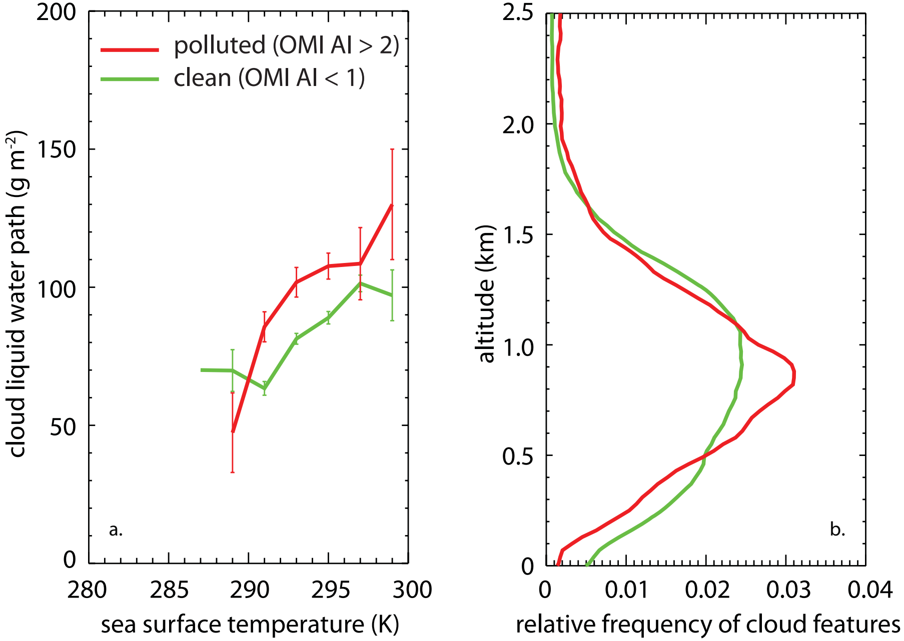

Fig. 5. **(a)** AMSR-E cloud liquid water path against AMSR-E sea surface temperature and **(b)** relative frequency of occurrence of CALIPSO cloud features. Both are shown separately for high smoke (red) and low smoke (green) samples. Vertical bars in (a) are the estimated 95% confidence interval based on variability in each SST bin. The total number of clean and polluted CALIPSO cloud features between 0 and 2.5 km altitude are 5 300 382 and 1 540 959, respectively.

ACPD
10, 18635–18659, 2010